Applied Catalysis A: General 443–444 (2012) 207–213

Contents lists available at SciVerse ScienceDirect

Applied Catalysis A: General

journal homepage: www.elsevier.com/locate/apcata

Tungstophosphoric acid/zirconia composites prepared by the sol–gel method: An efficient and recyclable green catalyst for the one-pot synthesis of 14-aryl-14*H*-dibenzo[*a*,*j*]xanthenes

Toa S. Rivera, Alexis Sosa, Gustavo P. Romanelli, Mirta N. Blanco, Luis R. Pizzio*

Centro de Investigación y Desarrollo en Ciencias Aplicadas "Dr. Jorge J. Ronco" (CINDECA), Departamento de Química, Facultad de Ciencias Exactas, UNLP-CCT La Plata, CONICET, 47 No 257, B1900AJK La Plata, Argentina

ARTICLE INFO

Article history:
Received 16 April 2012
Received in revised form 31 July 2012
Accepted 1 August 2012
Available online 10 August 2012

Keywords:
Mesoporous zirconia
Heteropolyacids
14-Aryl-14*H*-dibenzo[*a*,*j*]xanthenes
Heterogeneous catalysis
Solvent-free reaction

ABSTRACT

Samples of zirconia modified with different contents of tungstophosphoric acid (TPA) were synthesized from zirconium propoxide via sol–gel reactions using polyethylene glycol as template and were characterized by different physicochemical techniques (BET, XRD, FT-IR, and ^{31}P MAS-NMR). The S_{BET} of the solids decreases and the microporosity increases with the increase of the TPA content. According to FT-IR and ^{31}P MAS-NMR studies, the main species present in the samples is $[PW_{12}O_{40}]^{3-}$ anion, which was partially transformed into $[P_2W_{21}O_{71}]^{6-}$ and $[PW_{11}O_{39}]^{7-}$ anions during the synthesis and drying steps. The XRD patterns of the modified samples exhibit neither the characteristic peaks of TPA nor those attributed to its decomposition products.

Aryl-14*H*-dibenzo[*a*,*j*]xanthenes have been synthesized by a one-pot condensation of 2-naphthol and aryl aldehydes, catalyzed by tungstophosphoric acid/zirconia composites in a solvent-free medium using conventional heating. The present approach offers the advantages of clean reaction, simple methodology, short reaction time, and high yield. The reaction work-up is very simple and the catalyst can be easily separated from the reaction mixture and reused several times in subsequent reactions without appreciable loss of the catalytic activity.

1. Introduction

Organic reactions catalyzed by inorganic solid materials are gaining much importance due to the advantages of heterogeneous catalysis, such as simplified product isolation, mild reaction conditions, easy recovery and catalyst reuse, and reduction of waste by-products [1–3].

In particular, catalysis by heteropolyacids (HPA) and related compounds is a field of increasing significance worldwide. Many developments have been carried out both in basic research and in fine chemistry processes [4]. HPA have been used as valuable and versatile acid catalysts for some acid-catalyzed reactions because of their strong acidic properties [5,6]. They can be used as bulk or supported materials in both homogeneous and heterogeneous systems. Furthermore, HPA have several advantages, such as much flexibility in the modification of the acid strength, ease of handling, nontoxicity and environmental compatibility [7].

Zirconium oxide (zirconia) is an interesting material to be used as catalyst support due to its thermal stability, and its basic and acid properties. The latter can be modified by the addition of cationic or anionic substances. For example, the addition of sulfate or tungstate ions has been widely studied, obtaining materials with high acidity [8,9]. However, the addition of Keggin heteropolyacids has not been studied so much [10–14]. The most common methods to obtain zirconia are: sol–gel, micellar or mechanochemical synthesis [15]. The preparation of HPA supported on zirconia employing the micellar method, with zirconyl chloride as oxide precursor, has been more extensively reported than the sol–gel method using a zirconium alkoxide [13]. In addition, different types of ionic and neutral surfactants have been employed to obtain mesoporous materials with high specific surface area. More recently, nonsurfactant, low-cost organic compounds, such as urea, have started to be used as pore-forming agents [16].

Conversely, the preparation of organic compounds involving greener processes under solvent-free conditions has been investigated worldwide due to stringent environmental regulations. The implementation of several transformations in a single operation is highly compatible with the principles of Green Chemistry [17–19].

Xanthenes and benzoxanthenes are interesting compounds for the pharmaceutical industry due to their wide range of biological and therapeutic properties [20], such as anti-inflammatory, antibacterial, antiviral, and stimulating activity of the central

* Corresponding author. Fax: +54 221 4211353.
E-mail address: lrpizzio@quimica.unlp.edu.ar (L.R. Pizzio).

0926-860X/$ – see front matter © 2012 Elsevier B.V. All rights reserved.
http://dx.doi.org/10.1016/j.apcata.2012.08.001

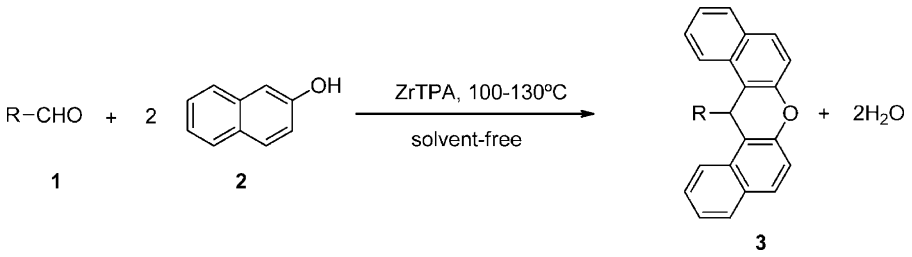

Scheme 1. Synthesis of 14-aryl-14*H*-dibenzo[*a*,*j*]xanthenes with TPA/zirconia composites as catalyst.

nervous system [21–24]; they are also used in photodynamic therapy [25] and for antagonism of the paralyzing action of zoxazolamine [26].

Different routes have been reported for the synthesis of xanthenes and benzoxanthenes, such as the reaction of aryl oxomagnesium halides with triethylorthoformate, trapping of benzynes by phenols, cyclization of polycyclic aryltriflate esters, and cyclocondensation between 2-hydroxy aromatic aldehydes and tetralone [27–30]. However, one of the best routes is the synthesis of 14-aryl-14*H*-dibenzo[*a*,*j*]xanthenes from 2-naphthol and aldehydes in the presence of a catalyst [31] such as AcOH-H_2SO_4, *p*-TSA, Amberlist-15, silica-sulfuric acid, and bulk or silica-supported heteropolyacids [32–37].

But, although these methods showed different degrees of success, some of them had limitations, such as large reaction times, low yields, use of toxic solvents, and harsh reaction conditions [37,38]; that is why the development of alternative clean procedures for the synthesis of benzoxanthenes and related compounds is a challenge. In this regard, our research group has experience in the friendly synthesis of heterocyclic compounds using HPA, such as coumarins, dihydropyrimidinones, azlactones, and flavones [39–42].

Continuing with the studies directed toward the development of highly expedient methods and the synthesis of diverse heterocyclic compounds, we are herein reporting a new one-pot synthesis of 14-aryl-14*H*-dibenzo[*a*,*j*]xanthenes from aldehydes and 2-naphthol under solvent-free conditions (Scheme 1), catalyzed by tungstophosphoric acid-modified mesoporous zirconia obtained from zirconium propoxide as precursor and polyethylene glycol as pore-forming agent.

2. Experimental

2.1. Catalyst preparation

Zirconium propoxide (Aldrich, 26.6 g) was mixed with absolute ethanol (Merck, 336.1 g) and stirred for 10 min to obtain a homogeneous solution under N_2 at room temperature. Then 0.47 cm^3 of 0.28 M HCl aqueous solution was dropped slowly into the above mixture to catalyze the sol–gel reaction.

After 3 h, an appropriate amount of polyethylene glycol (PEG)–alcohol–water solution (1:5:1 weight ratio) was added to the hydrolyzed solution under vigorous stirring to act as template. The amount of added solution was fixed in order to obtain a template concentration of 10% by weight in the final material. A tungstophosphoric acid $H_3PW_{12}O_{40}{\cdot}6H_2O$ (TPA) solution, whose concentration was varied in order to obtain a TPA concentration of 30% and 60% w/w in the solid, was added together with the template addition (ZrTPA30B and ZrTPA60B samples) and also after 24 h of the gel aging (ZrTPA30A and ZrTPA60A samples). A sample without TPA addition was obtained with the aforementioned procedure (ZrTPA00A).

The gels were then kept in a beaker at room temperature up to dryness. The solids were ground into powder and extracted with distilled water for three periods of 8 h, in a system with continuous stirring, to remove PEG. Afterwards, the solids were calcined at 100 °C for 24 h.

2.2. Catalyst characterization

The specific surface area and the mean pore diameter of the solids were determined from the N_2 adsorption–desorption isotherms at the liquid–nitrogen temperature, obtained using Micromeritics ASAP 2020 equipment. The solids were previously degassed at 100 °C for 2 h.

The X-ray diffraction (XRD) patterns were recorded with Philips PW-1732 equipment with a built-in recorder, using Cu Kα radiation, nickel filter, 20 mA and 40 kV in the high voltage source, and scanning angle between 5° and 60° 2θ at a scanning rate of 1° per min.

The ^{31}P magic angle spinning-nuclear magnetic resonance (^{31}P MAS-NMR) spectra were recorded with Bruker Avance II equipment, using the CP/MAS ^{1}H–^{31}P technique. A sample holder of 4 mm diameter and 10 mm in height was employed, using 5 μs pulses, a repetition time of 4 s, and working at a frequency of 121.496 MHz for ^{31}P at room temperature. The spin rate was 8 kHz and several hundred pulse responses were collected. Phosphoric acid 85% was employed as external reference.

The Fourier transform infrared (FT-IR) spectra of the solids were obtained using a Bruker IFS 66 FT-IR spectrometer and pellets in KBr in the 400–4000 cm^{-1} wavenumber range.

The acidity of the solids was estimated by means of potentiometric titration. A known mass of solid was suspended in acetonitrile and stirred for 3 h. Then, the suspension was titrated with 0.05 N n-butylamine in acetonitrile using Metrohm 794 Basic Titrino apparatus with a double junction electrode.

2.3. Synthesis of aryl-14H-dibenzo[a,j]xanthenes

All chemical reagents were obtained from Aldrich and were used without further purification. All products were identified by comparison of their physical and spectral data with those of the authentic samples. Melting points were measured using a Bioamerican Bs 448 apparatus and are uncorrected. ^{1}H NMR and ^{13}C NMR spectra were recorded with a Varian 200 MHz (see Supplementary data). The purity of the substances and the progress of the reaction were monitored by TLC on silica gel, and yields refer to isolated products.

A mixture of the aldehyde (1.2 mmol), 2-naphthol (2 mmol) and the catalyst (50 mg TPA) was stirred at 130 °C for the desired time. The reaction mixture was cooled to 25 °C, then toluene (5 cm^3) was added, and the mixture was stirred for 15 min before being filtered to separate the catalyst. It was washed twice with toluene (3 cm^3). The combined toluene extracts were washed twice with water (5 cm^3), dried over anhydrous Na_2SO_4 and evaporated in vacuo. The obtained solid was recrystallized from ethyl alcohol to afford the pure 14-aryl-14*H*-dibenzo[*a*,*j*]xanthene derivative.

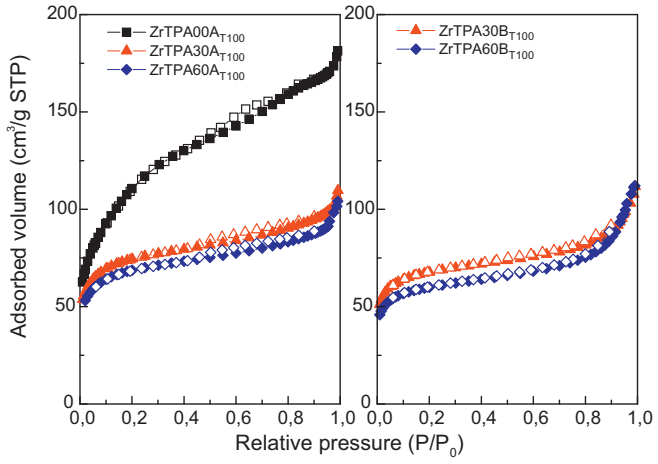

Fig. 1. N_2 adsorption–desorption isotherms of ZrTPA00A$_{T100}$, ZrTPA30A$_{T100}$, ZrTPA60A$_{T100}$, ZrTPA30B$_{T100}$, and ZrTPA60B$_{T100}$ samples. Adsorption branch (full symbols), desorption branch (open symbols).

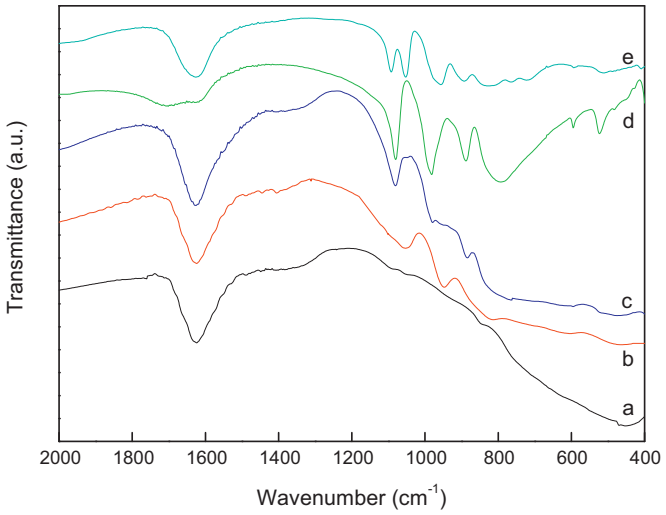

Fig. 2. FT-IR spectra of ZrTPA00A$_{T100}$ (a), ZrTPA30A$_{T100}$ (b), and ZrTPA60A$_{T100}$ (c) samples; bulk TPA (d), and sodium salt of $[PW_{11}O_{39}]^{7-}$ anion (e).

3. Results and discussion

3.1. Catalyst characterization

The textural properties of the samples were determined from the N_2 adsorption–desorption isotherms at the liquid–nitrogen temperature. The isotherms obtained (Fig. 1) showed the main characteristics assigned to mesoporous materials and can be classified as type IV. The hysteresis was hardly visible, which is attributed to an ordered arrangement of the mesopores present in the material, as was reported for MCM-41 and mesoporous titania modified with tungstophosphoric acid [43,44].

The specific surface area (S_{BET}) of the samples determined from the N_2 adsorption–desorption isotherms using the Brunauer–Emmett–Teller (BET) method, the average pore diameter (D_p), and the micropore specific surface area (S_{Micro}) estimated from the t-plot method are listed in Table 1.

The sample obtained without TPA addition (ZrTPA00A$_{T100}$) is a mesoporous solid and has the highest specific surface area. When TPA was added, S_{BET} decreased and the microporosity (S_{Micro}) increased; these effects were slightly higher when TPA was added immediately after PEG (samples ZrTPA30B$_{T100}$, ZrTPA60B$_{T100}$).

The S_{BET} decrease that takes place with a higher TPA amount (Table 1) can be attributed to a decrease in the cross-linking degree during the sol–gel synthesis when the acid concentration is increased. This is in agreement with reports in the literature that indicate a similar behavior for the specific surface of mesoporous titania obtained via the sol–gel process [45,46].

The XRD patterns of the ZrTPA00A$_{T100}$ showed a broad band at $2\theta = 30^\circ$ attributed to its low crystallinity. On the other hand, the XRD patterns of the samples modified with TPA displayed the same broad band. Diffraction lines attributed to crystalline TPA or its decomposition products were not observed, indicating that TPA is highly dispersed in the zirconia matrix.

The FT-IR spectrum of the ZrTPA00A$_{T100}$ sample (Fig. 2) displayed an intense band between 3600 and 3200 cm^{-1} and another one at 1600 cm^{-1}, assigned to the stretching vibrations of hydroxo- and aquo-OH, and to the bending vibration of (H–O–H) and (O–H–O) present in the structure of the solid, respectively [47–49]. Also, in the energy interval below 850 cm^{-1}, the wide band due to Zr–O stretching vibration was observed.

The FT-IR spectrum of TPA (Fig. 2) showed bands at 1081, 982, 888, 793, 595, and 524 cm^{-1}, which are in agreement with those reported in the literature for the $H_3PW_{12}O_{40}$ acid [50]. The first five bands are assigned to the stretching vibrations P–O$_a$, W–O$_d$, W–O$_b$–W, W–O$_c$–W, and to the bending vibration O$_a$–P–O$_a$, respectively. The subscripts indicate oxygen bridging W and the P heteroatom (a), corner sharing (b) and edge sharing (c) oxygen belonging to WO_6 octahedra, and terminal oxygen (d).

As a result of the addition of TPA to the zirconia matrix, the FT-IR spectra of the ZrTPA30A$_{T100}$, ZrTPA60A$_{T100}$ (Fig. 2), ZrTPA30B$_{T100}$, and ZrTPA60B$_{T100}$ samples displayed a new set of bands overlapped to the zirconia wide band. The presence of the P–O$_a$, W–O$_d$, and W–O$_b$–W stretching vibrations of the $[PW_{12}O_{40}]^{3-}$ anion can be clearly observed (ZrTPA60A$_{T100}$ and ZrTPA60B$_{T100}$ samples). In addition, bands assigned to the $[PW_{11}O_{39}]^{7-}$ anion are also observed in the ZrTPA30A$_{T100}$ and ZrTPA30B$_{T100}$ samples if a comparison with the spectrum of the sodium salt of the lacunary anion is made, which presents bands at 1100, 1046, 958, 904, 812, and 742 cm^{-1} (Fig. 2), in agreement with the literature [50].

On the other hand, the FT-IR spectra of the samples after being leached with distilled water did not present any of the characteristic bands of PEG, such as that assigned to the C–O stretching mode of the ether group of PEG at 1099 cm^{-1} [51], showing that the template removal by water extraction was effective.

^{31}P MAS-NMR spectra of ZrTPA30A$_{T100}$, ZrTPA60A$_{T100}$, ZrTPA30B$_{T100}$, and ZrTPA60B$_{T100}$ samples are shown in Fig. 3. For the ZrTPA60A$_{T100}$ and ZrTPA60B$_{T100}$ samples, the spectra displayed a wide band with a maximum at around −14 ppm, accompanied by a shoulder at −12 ppm. They may be attributed to the $[PW_{12}O_{40}]^{3-}$ anion and to the $[P_2W_{21}O_{71}]^{6-}$ dimeric species, respectively [52]. The downfield shift and the increase of the line width observed, compared to the TPA (−15.3 ppm), can be attributed to the interaction between the anion and the zirconia matrix [53]. The interaction can be assumed to be of the

Table 1
Textural properties of the solids calcined at 100 °C.

Sample	S_{BET} (m^2/g)	S_{Micro}[a] (m^2/g)	D_P[b] (nm)
ZrTPA00A$_{T100}$	396	6	2.8
ZrTPA30A$_{T100}$	265	157	2.5
ZrTPA60A$_{T100}$	230	134	2.4
ZrTPA30B$_{T100}$	243	160	3.4
ZrTPA60B$_{T100}$	213	140	3.6

[a] Micropore specific surface area estimated by the *t*-plot method.
[b] Mean pore diameter obtained from the specific BET surface area.

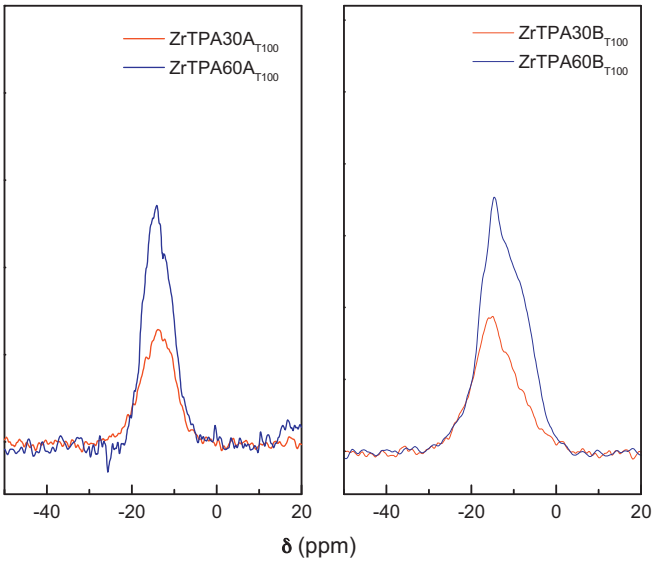

Fig. 3. ^{31}P MAS-NMR spectra of ZrTPA30A$_{T100}$, ZrTPA60A$_{T100}$, ZrTPA30B$_{T100}$, and ZrTPA60B$_{T100}$ samples.

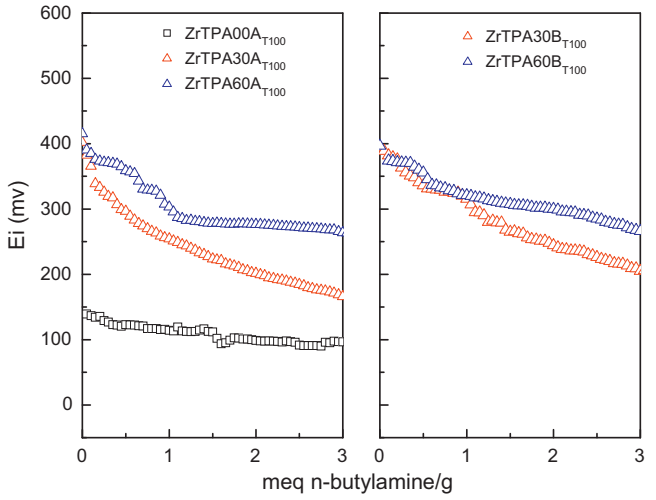

Fig. 4. Potentiometric titration curves of ZrTPA00A$_{T100}$, ZrTPA30A$_{T100}$, ZrTPA60A$_{T100}$, ZrTPA30B$_{T100}$, and ZrTPA60B$_{T100}$ samples.

electrostatic type due to the transfer of protons to Zr–OH [54] according to:

$$Zr\text{–}OH + H_3PW_{12}O_{40} \rightarrow [Zr\text{–}OH_2^+]_n[H_{3-n}PW_{12}O_{40}]^{-n}$$

However, the adsorption might not even be purely electrostatic involving, in addition, interactions of hydrogen bond type between oxygen atoms of TPA species and hydroxyl groups of the zirconia matrix.

On the other hand, the ^{31}P MAS-NMR spectra of ZrTPA30A$_{T100}$ and ZrTPA30B$_{T100}$ also showed the wide band with a shoulder assigned to the $[PW_{12}O_{40}]^{3-}$ and $[P_2W_{21}O_{71}]^{6-}$ species.

According to FT-IR and ^{31}P MAS-NMR results, the main species present in the samples is the $[PW_{12}O_{40}]^{3-}$ anion. However, it was partially transformed into $[P_2W_{21}O_{71}]^{6-}$ and $[PW_{11}O_{39}]^{7-}$ anions during the synthesis and drying steps. This transformation is due to the limited stability range of the $[PW_{12}O_{40}]^{3-}$ anion in solution. At pH 1.5–2, it is reversibly and quickly transformed into the lacunar species $[PW_{11}O_{39}]^{7-}$. Pope [55] has proposed the following transformation scheme: $[PW_{12}O_{40}]^{3-} \Leftrightarrow [P_2W_{21}O_{71}]^{6-} \Leftrightarrow [PW_{11}O_{39}]^{7-}$ when the hydroxyl concentration is increased. This may be considered as a valid path followed by the TPA species during the synthesis of the samples.

The acidity measurements of the catalysts by means of potentiometric titration with n-butylamine let us estimate the number of acid sites and their acid strength. It was suggested that the initial electrode potential (E_i) indicates the maximum acid strength of the sites and the value of meq amine/g solid where the plateau is reached indicates the total number of acid sites. The acid strength of these sites may be classified according to the following scale: $E_i > 100$ mV (very strong sites), $0 < E_i < 100$ mV (strong sites), $-100 < E_i < 0$ (weak sites), and $E_i < -100$ mV (very weak sites) [56,57].

The acid strength of the modified samples ZrTPA30A$_{T100}$ (E_i = 402 mV), ZrTPA60A$_{T100}$ (E_i = 415 mV), ZrTPA30B$_{T100}$ (E_i = 394 mV) and ZrTPA60B$_{T100}$ (E_i = 397 mV) was markedly higher than that of the unmodified ZrTPA00A$_{T100}$ (E_i = 140 mV) (Fig. 4.) but lower than that of bulk TPA (E_i = 620 mV) [58]. However, they were almost independent of the TPA concentration and the time elapsed between the template PEG solution addition and the TPA incorporation. The lower acid strength of the ZrTPA samples compared to bulk TPA could be assigned to the fact that the protons in the $H_3PW_{12}O_{40}{\cdot}6H_2O$ are present as $H^+(H_2O)_2$ species, whereas in the ZrTPA samples they are interacting with the oxygen of Zr–OH groups or in a higher hydration state ($H^+(H_2O)_n$). This is in agreement with previous work [58] reporting that the $H_3PW_{12}O_{40}{\cdot}21H_2O$, where the protons are highly hydrated, displayed lower acid strength (E_i = 538 mV) than $H_3PW_{12}O_{40}{\cdot}6H_2O$, while the partially substituted salts $Cs(K)_{2.9}H_{0.1}PW_{12}O_{40}$ containing bare protons showed E_i in the range 900–1000 mV.

On the other hand, the number of acid sites determined by potentiometric titration increased with the increment of the TPA content and followed the order: ZrTPA30A$_{T100}$ < ZrTPA30B$_{T100}$ < ZrTPA60A$_{T100}$ < ZrTPA60B$_{T100}$.

3.2. Catalytic tests

To study the synthesis of 14-phenyl-14*H*-dibenzo[*a*,*j*]xanthene, blank experiments without the presence of catalyst were initially conducted. In order to obtain the optimal reaction temperature, four temperatures (80, 100, 120, and 130 °C) were tested. The experimental reaction conditions were: 1.2 mmol of benzaldehyde, 2 mmol of 2-naphthol, solvent-free conditions, and a reaction time of 1.5 h. No reaction was observed at 80 and 100 °C (Table 2, entries 1 and 2). A temperature increase gave low substrate conversion. The yield of 14-phenyl-14*H*-dibenzo[*a*,*j*]xanthene at 120 °C was only 15% (Table 2, entry 3), whereas at 130 °C the conversion was 32% (Table 2, entry 4), which was almost the same for a reaction time of 5 h (Table 2, entry 5).

Afterwards, the catalytic activity of bulk TPA was tested in the preparation of 14-phenyl-14*H*-dibenzo[*a*,*j*]xanthene. The results are listed in Table 3. The experimental reaction conditions were the same as those mentioned above, but 50 mg (1.7 mmol TPA % with respect to the aldehyde) was added and the reaction time

Table 2
Effect of reaction temperature on xanthene yield for blank experiments.

Entry	Temperature (°C)	Yield[a] (%)
1	80	–
2	100	–
3	120	15
4	130	32
5	130[b]	30

Reaction conditions: benzaldehyde, 1.2 mmol; 2-naphthol, 2 mmol; time, 1.5 h.
[a] Isolated yield.
[b] Reaction time: 5 h.

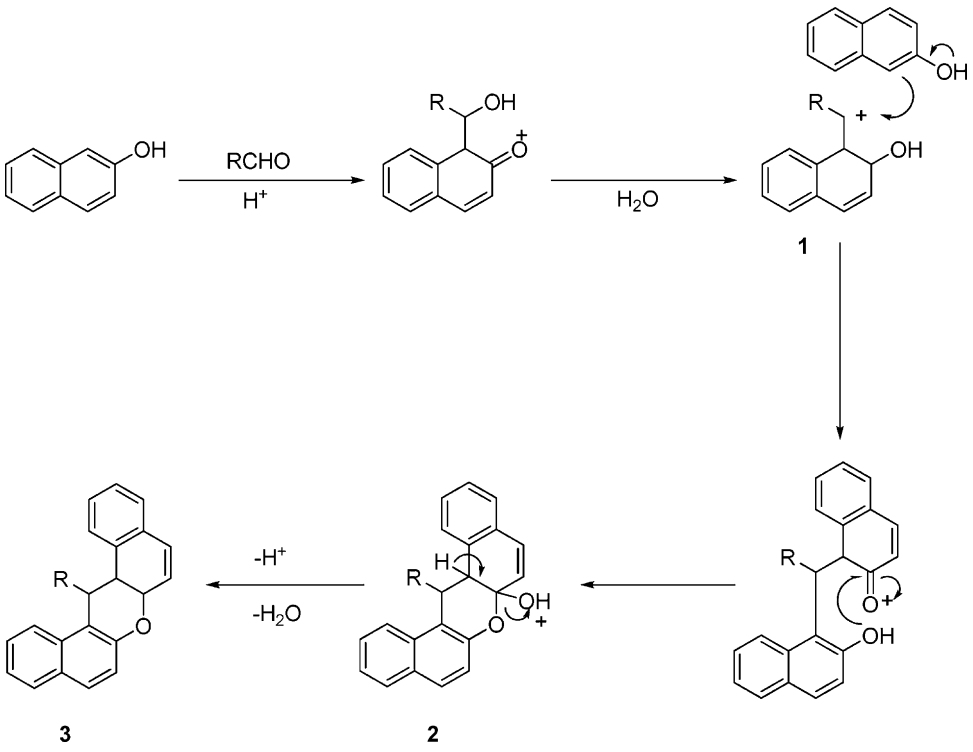

Scheme 2. Plausible reaction mechanism for the formation of 14-aryl-14*H*-xanthenes based on a previous report [20].

was 1 h. No reaction was detected at 80 °C, even at a reaction time of 3 h. Only traces of the product were obtained at 100 °C (Table 3, entry 2), though following the reaction up to 3 h, a low yield was obtained (Table 3, entry 3). The yield of 14-phenyl-14*H*-dibenzo[*a*,*j*]xanthene increased notably to 78% at 130 °C (Table 3, entry 4).

Then, the catalytic activity of the mesoporous zirconia modified with tungstophosphoric acid (ZrTPA30A$_{T100}$, ZrTPA60A$_{T100}$, ZrTPA30B$_{T100}$, and ZrTPA60B$_{T100}$ samples) in the preparation of 14-phenyl-14*H*-dibenzo[*a*,*j*]xanthene was studied. The results are listed in Table 4. The reaction was carried out under solvent-free conditions, using 1.2 mmol of benzaldehyde, 2 mmol of 2-naphthol, and 1.7 mmol TPA % in the catalyst. No reaction was observed at 80 °C, even at a reaction time of 3 h, and a yield of product lower than 10% was obtained at 100 °C for a reaction time of 3 h (Table 4, entries 1 and 2). As was observed using bulk TPA as catalyst, the yield of 14-phenyl-14*H*-dibenzo[*a*,*j*]xanthene increased notably for the reaction performed at 130 °C.

The samples with higher content of TPA (ZrTPA60A$_{T100}$ and ZrTPA60B$_{T100}$) showed the best yields (Table 4, entry 3). On the other hand, the yields obtained using ZrTPA30A$_{T100}$ and ZrTPA30B$_{T100}$ were slightly lower. Additionally, their yields were almost independent of the time elapsed between the additions of the template PEG solution and TPA.

Despite their lower acid strength, the ZrTPA samples displayed higher catalytic activity than the bulk TPA. This is assigned to the high specific surface area of the TPA/zirconia composites (265–213 m^2/g), which allows us to obtain materials with a higher amount of protons exposed on the surface than bulk TPA (2 m^2/g). This is in agreement with the fact that ZrTPA60A$_{T100}$ and ZrTPA60B$_{T100}$ samples, with a slightly higher number of acid sites determined by potentiometric titration, have displayed higher yields in the synthesis of 14-phenyl-14*H*-dibenzo[*a*,*j*]xanthenes.

It must be pointed out that under these experimental reaction conditions, using the unmodified ZrTPA00$_{T100}$ sample as catalyst, a 30% yield was obtained, which is similar to the value obtained in the blank experiments.

Table 3
Effect of reaction temperature on xanthene yield using bulk TPA as catalyst.

Entry	Temperature (°C)	Time (h)	Yield[a] (%)
1	80	3	–
2	100	1	Traces
3	100	3	10
4	130	1	78

Reaction conditions: benzaldehyde, 1.2 mmol; 2-naphthol, 2 mmol; catalyst amount, 50 mg TPA.
[a] Isolated yield.

Table 4
Effect of reaction temperature on xanthene yield using TPA/zirconia composites as catalyst.

Entry	Temperature (°C)	Time (h)	Yield[a] (%)			
			ZrTPA30A$_{T100}$	ZrTPA60A$_{T100}$	ZrTPA30B$_{T100}$	ZrTPA60B$_{T100}$
1	80	3	–	–	–	–
2	100	3	6	9	8	10
3	130	1	85	95	88	99

Reaction conditions: benzaldehyde, 1.2 mmol; 2-naphthol, 2 mmol; catalyst amount, 170 mg (samples ZrTPA30A$_{T100}$ and ZrTPA30B$_{T100}$) or 85 mg (samples ZrTPA60A$_{T100}$ and ZrTPA60B$_{T100}$).
[a] Isolated yield.

Table 5
Effect of reusability of ZrTPA60B$_{T100}$ catalyst on the xanthene yield.

Entry	Cycle	Yield[a] (%)
1	0	99
2	1	98
3	2	98
4	3	96

Reaction conditions: benzaldehyde, 1.2 mmol; 2-naphthol, 2 mmol; catalyst amount, 170 mg; temperature, 130 °C; time, 1 h.
[a] Isolated yield.

Table 6
Synthesis of 14-aryl-14*H*-dibenzo[*a*,*j*]xanthenes with ZrTPA60B$_{T100}$ as catalyst.

Entry	Aromatic aldehyde	Time (h)	Yield[a] (%)
1	Benzaldehyde	1	99
2	4-Methylbenzaldehyde	1	94
3	4-Methoxybenzaldehyde	1	93
4	4-Florobenzaldehyde	2	98
5	4-Chlorobenzaldehyde	2	96
6	2,4,6-Trimethoxybenzaldehyde	5	60
7	2-Naphthaldehyde	3	78

Reaction conditions: aldehyde, 1.2 mmol; 2-naphthol, 2 mmol; catalyst amount, 85 mg; temperature, 130 °C.
[a] Isolated yield.

The reusability of the catalyst was checked using the ZrTPA60B$_{T100}$ sample, by separating the solid from the reaction mixture by simple filtration, washing with toluene, and drying in vacuum oven at room temperature for 4 h prior to reuse in subsequent reactions. No significant loss in the product yield was observed (Table 5).

After the best reaction conditions were achieved, the generality of these conditions to other substrates was studied, employing ZrTPA60B$_{T100}$ as catalyst. Using this method, different kinds of aromatic compounds were reacted with 2-naphthol to produce the corresponding 14-aryl-14*H*-dibenzo[*a*,*j*]xanthenes at 130 °C under solvent-free conditions. The results are summarized in Table 6. Several aromatic aldehydes with different functional groups were subjected to the condensation reaction, and the desired products were synthesized in good to excellent yields. The substituted functional groups in the aromatic ring of the aldehyde affect the yield and the reaction time in two cases. In comparison with electron-withdrawing groups in the aldehyde, it was found that the presence of electron-donating groups in the aldehyde decreased both the reaction rate and the yield of products (Table 6, entries 6 and 7).

A mechanistic rationale portraying the probable sequence of events is given in Scheme 2. The reaction likely proceeds via the initial formation of the carbocation (**1**). The oxonium species (**2**) is then formed on reaction with 2-naphthol, which then undergoes dehydration to afford the desired product (**3**).

It must be remarked that for all the studied reactions the products were selectively obtained, without the formation of by-products.

4. Conclusions

Tungstophosphoric acid/zirconia composite materials were prepared using PEG as pore-forming agent, via sol–gel reactions.

FT-IR and ^{31}P MAS-NMR results indicated that the main species present in the samples is the $[PW_{12}O_{40}]^{3-}$ anion, which was partially transformed into $[P_2W_{21}O_{71}]^{6-}$ and $[PW_{11}O_{39}]^{7-}$ anions during the synthesis and drying steps. The prepared catalysts presented acid and textural properties adequate for their use as catalysts in heterogeneous acid reactions.

ZrTPA composites have proved to be a very efficient catalyst for the synthesis of dibenzoxanthene derivatives. A convenient and green process for the synthesis of aryl-14*H*-dibenzo[*a*,*j*]xanthenes by condensation of various aromatic aldehydes with 2-naphthol using ZrTPA as a heterogeneous acid catalyst in solvent-free conditions, using conventional heating at 130 °C, has been developed. Additionally, short reaction times, excellent yields, straightforward procedure, and relative nontoxicity of the catalyst are other noteworthy advantages of this method. Finally, these solid acid catalysts can be recovered and reused at least four times with negligible loss in their activity.

Acknowledgements

The authors thank ANPCyT, CONICET and Universidad Nacional de La Plata, for financial support, and L. Soto, L. Osiglio, D. Peña and N. Firpo for their collaboration in the experimental measurements.

Appendix A. Supplementary data

Supplementary data associated with this article can be found, in the online version, at http://dx.doi.org/10.1016/j.apcata.2012.08.001.

References

[1] J. Clark, Acc. Chem. Res. 35 (2002) 791–797.
[2] T. Okuhara, Chem. Rev. 102 (2002) 3641–3666.
[3] K. Wilson, J.H. Clark, Pure Appl. Chem. 72 (2000) 1313–1319.
[4] M. Misono, N. Nojiri, Appl. Catal. A: Gen. 64 (1990) 1–30.
[5] M. Amini, M. Seyyedhamzeh, A. Bazgir, Appl. Catal. A: Gen. 323 (2007) 242–245.
[6] I. Kozhevnikov, J. Mol. Catal. A: Chem. 262 (2007) 86–92.
[7] I. Kozhevnikov, Chem. Rev. 98 (1998) 171–198.
[8] G. Yadav, J. Nair, Micropor. Mesopor. Mater. 33 (1999) 1–48.
[9] R. Boyse, E. Ko, J. Catal. 171 (1997) 191–207.
[10] E. López-Salinas, J.G. Hernández-Cortéz, M.A. Cortés-Jácome, J. Navarrete, M.E. Llanos, A. Vázquez, H. Armendáriz, T. López, Appl. Catal. A: Gen. 175 (1998) 43–53.
[11] B. Devassy, G. Shanbhag, S. Halligudi, J. Molec. Catal. A: Chem. 247 (2006) 162–170.
[12] S. Mallik, S. Dash, K. Parida, B. Mohapatra, J. Colloid Interface Sci. 300 (2006) 237–243.
[13] X. Qu, Y. Guo, Ch Hu, J. Molec. Catal. A: Chem. 262 (2007) 128–135.
[14] L. Pizzio, P. Vázquez, C. Cáceres, M. Blanco, Catal. Lett. 77 (2001) 233–239.
[15] M. Fernández-García, A. Martínez-Arias, J. Hanson, J. Rodríguez, Chem. Rev. 104 (2004) 4063–4104.
[16] M.N. Gorsd, M.N. Blanco, L.R. Pizzio, Stud. Surf. Sci. Catal. 175 (2010) 405–408.
[17] R. Kumar, G. Nandi, R. Verma, M. Singh, Tetrahedron Lett. 51 (2010) 442–445.
[18] A. Rahmati, Chin. Chem. Lett. 21 (2010) 761–764.
[19] R. Kumar, G. Nandi, R. Verna, M. Singh, Tetrahedron Lett. 51 (2010) 442–445.
[20] J. Madhav, Y. Reddy, P. Reddy, M. Reddy, S. Kuarm, P. Crooks, B. Rajitha, J. Mol. Catal. A: Chem. 304 (2009) 85–87.
[21] K. Chibale, M. Visser, D. Schalkwyk, P. Smith, A. Saravanamuthu, A. Fairlamb, Tetrahedron 59 (2003) 2289–2296.
[22] A. El-Brashy, M. Metwally, F. El-Sepai, Farmaco 59 (2004) 809–817.
[23] J. Jamison, K. Krabill, A. Hatwalkar, Cell. Biol. Int. Rep. 14 (1990) 1075–1084.
[24] J. Lewis, M. Readhead, J. Med. Chem. 13 (1970) 525–527.
[25] R. Ion, Prog. Catal. 2 (1997) 55–76.
[26] G. Saint-Ruf, A. De, H. Hieu, Bull. Chim. Ther. 7 (1972) 83–86.
[27] G. Cusiragui, G. Cusnati, M. Cornia, Tetrahedron Lett. 14 (1973) 679–682.
[28] D. Knight, P. Little, J. Chem. Soc., Perkin Trans. I 14 (2001) 1771–1777.
[29] J. Wang, R. Harrey, Tetrahedron 58 (2002) 5927–5931.
[30] A. Jha, J. Beal, Tetrahedron Lett. 45 (2004) 8999–9001.
[31] B. Mirjalili, A. Bamoniri, A. Akbari, Chim. Chem. Lett. 22 (2011) 45–48.
[32] R. Sharma, J. Baruah, Dyes Pigments 64 (2005) 91–92.
[33] A. Khosropour, M. Khodaei, H. Moghannian, Synlett (2005) 955–958.
[34] S. Ko, C. Yao, Tetrahedron Lett. 47 (2006) 8827–8829.
[35] S. Mozhdeh, M. Peiman, A. Bazgir, Dyes Pigments 76 (2008) 836–839.
[36] L. Nagarapu, S. Kantevari, V. Mahankhali, S. Apuri, Catal. Commun. 8 (2007) 1173–1177.
[37] M. Amini, M. Seyyedhamzeh, A. Bazgir, Appl. Catal. A: Gen. 323 (2007) 242–245.
[38] R. Kumar, G. Nandi, R. Verna, M. Singh, Tetrahedron Lett. 51 (2010) 442–445.
[39] G. Romanelli, D. Bennardi, D. Ruiz, G. Baronetti, H. Thomas, J. Autino, Tetrahedron Lett. 45 (2004) 8935–8939.
[40] G. Romanelli, A. Sathicq, J. Autino, H. Thomas, G. Baronetti, Synth. Commun. 37 (2007) 3907–3916.
[41] G. Romanelli, J. Autino, P. Vaïzquez, L. Pizzio, M. Blanco, C. Caïceres, Appl. Catal. A: Gen. 352 (2009) 208–213.
[42] D. Bennardi, G. Romanelli, J. Autino, L. Pizzio, P. Vázquez, C. Cáceres, M. Blanco, React. Kinet. Mech. Catal. 100 (2010) 165–174.
[43] S. Ajaikumar, A. Pandurangan, J. Mol. Catal. A: Chem. 266 (2007) 1–10.

[44] V.M. Fuchs, E.L. Soto, M.N. Blanco, L.R. Pizzio, J. Colloid Interface Sci. 327 (2008) 403–411.
[45] N. Phonthammachai, T. Chairassameewong, E. Gulari, A.M. Jamieson, S. Wongkasemjit, Micropor. Mesopor. Mater. 66 (2003) 261–271.
[46] K.M.S. Khalil, T. Baird, M.I. Zaki, A.A. El-Samahy, A.M. Awad, Colloid Surf. A 132 (1998) 31–44.
[47] S. Patel, N. Purohit, A. Patel, J. Mol. Catal. A: Chem. 192 (2003) 195–202.
[48] J. Rubio, J.L. Otero, M. Villegas, P. Duran, J. Mater. Sci. 32 (1997) 643–652.
[49] J.A.R. Van Veen, F.T.G. Veltmaat, G. Jonkers, J. Chem. Soc., Chem. Commun. (1985) 1656–1658.
[50] C. Rocchiccioli-Deltcheff, R. Thouvenot, R. Franck, Spectrochim. Acta 32A (1976) 587–597.
[51] D.-H. Jung, Y.K. Ko, H.-T. Jung, Mater. Sci. Eng. C 24 (2004) 117–121.
[52] R. Massart, R. Contant, J. Fruchart, J. Ciabrini, M. Fournier, Inorg. Chem. 16 (1977) 2916–2921.
[53] V.M. Mastikhin, S.M. Kulikov, A.V. Nosov, I.V. Kozhevnikov, I.L. Mudrakovsky, M.N. Timofeeva, J. Mol. Catal. A: Chem. 60 (1990) 65–70.
[54] E. López-Salinas, J.G. Hernández-Cortéz, I. Schifter, E. Torres-Garcıĭa, J. Navarrete, A. Gutiérrez-Carrillo, T. López, P.P. Lottici, D. Bersani, Appl. Catal. A: Gen. 193 (2000) 215–225.
[55] M.T. Pope, Heteropoly Isopoly Oxometalates, Springer-Verlag, Heidelberg, 1983, p. 180.
[56] R. Cid, G. Pecci, Appl. Catal. A: Gen. 14 (1985) 15–21.
[57] V.M. Fuchs, L.R. Pizzio, M.N. Blanco, Eur. Polym. J. 44 (2008) 801–807.
[58] L.R. Pizzio, M.N. Blanco, Appl. Catal. A: Gen. 255 (2003) 265–277.